Journal of Solid State Chemistry 184 (2011) 1977–1982

Contents lists available at ScienceDirect

Journal of Solid State Chemistry

journal homepage: www.elsevier.com/locate/jssc

Preparation and visible light photocatalytic activity of Bi_2O_3/Bi_2WO_6 heterojunction photocatalysts

Ming-Sheng Gui, Wei-De Zhang*, Qing-Xi Su, Cai-Hong Chen

School of Chemistry and Chemical Engineering, South China University of Technology, 381 Wushan Road, Guangzhou 510640, People's Republic of China

ARTICLE INFO

Article history:
Received 3 February 2011
Received in revised form
26 April 2011
Accepted 29 May 2011
Available online 6 June 2011

Keywords:
Heterojunction
Bismuth oxide
Bi_2WO_6
Photocatalytic activity
Rhodamine B

ABSTRACT

The Bi_2O_3/Bi_2WO_6 heterojunction photocatalysts were prepared by a two-step solvothermal process using $Bi(NO_3)_3$-ethylene glycol solution as Bi source. The catalysts were characterized by X-ray diffraction, scanning and transmission electron microscopy, X-ray photoelectron spectroscopy, and UV–vis diffuse reflection spectroscopy. The heterostructure catalysts are composed of Bi_2O_3 nanoparticles as modifier and 3D Bi_2WO_6 microspheres as substrate. Bi_2O_3 nanoparticles with diameters of about 10–15 nm are tightly grown on the lateral surface of the Bi_2WO_6 microspheres. The hierarchical Bi_2O_3/Bi_2WO_6 microspheres exhibit higher photocatalytic activity than the single phase Bi_2WO_6 or Bi_2O_3 for the degradation of rhodamine B under visible light illumination ($\lambda > 420$ nm). The enhancement of the photocatalytic activity of the Bi_2O_3/Bi_2WO_6 heterojunction catalysts can be ascribed to their improved light absorption property and the reduced recombination of the photoexcited electrons and holes during the photocatalytic reaction. The effect of loading amount of Bi_2O_3 on the catalytic performance of the heterojunction catalysts was also investigated and the optimal content of Bi_2O_3 is 3 wt%. The Bi_2O_3/Bi_2WO_6 heterojunction photocatalysts are essentially stable during the photocatalytic process.

1. Introduction

Since the discovery of photocatalytic splitting of water and photoinduced degradation of organic compounds by TiO_2 as a photocatalyst under UV light irradiation [1,2], various photocatalysts have been extensively developed in purifying water and air. However, this technique can hardly satisfy practical water treatment due to the rapid recombination of the photoexcited carriers and limited efficiency in visible light [3]. Therefore, it remains a great challenge to design efficient visible light-driven photocatalysts. In recent years, many strategies have been adopted to improve this situation. Besides doping semiconductor oxides with metals or non-metals for improving the photocatalytic activity [4], fabrication of heterostructured photocatalysts with different carriers or different band gaps has turned out to be an effective approach [5–7]. Among the semiconductive oxides, Bi_2O_3 has recently captured considerable attention due to its high refractive index, visible light activity, dielectric permittivity, and thermal stability [8]. Furthermore, Bi_2O_3 is a p-type semiconductor with suitable band edge potentials for water oxidation [9,10]. For example, Bi_2O_3/TiO_2 heterostructure could be easily activated by visible light owing to the photosensitization by Bi_2O_3 [11,12]. Similarly, $BiOCl/Bi_2O_3$, $Bi_2O_3/BaTiO_3$, and Bi_2O_3/NiO have shown greatly enhanced photocatalytic activity because of the efficient separation of photoexcited electrons and holes [5,13,14].

Being another important photocatalyst, Bi_2WO_6 has received particular attention recently because of its excellent photocatalytic property under visible light [15–18]. Unfortunately, its high efficiency of electron–hole recombination prohibits the desirable catalytic activity under visible light irradiation. Therefore, most studies have focused on improving its catalytic activity. One solution is to prepare 3D nanostructured catalysts with large specific surface area, for example, self-assembled three-dimensional hierarchical Bi_2WO_6 microspheres [19], hollow spheres [20,21], flower-like nanostructures [22–24], and so forth. Other efforts have been made on metal and non-metal doping, for example, doping of Bi_2WO_6 with F, N, and Ag, which showed improved photocatalytic performance [25–27].

Considering that Bi_2O_3 and Bi_2WO_6 can be constructed to heterojunction interface with matching band potentials (Bi_2O_3: $E_{CB}=0.33$, $E_{VB}=3.13$; Bi_2WO_6: $E_{CB}=046$, $E_{VB}=3.26$) [9,10,28,29], we prepared Bi_2O_3/Bi_2WO_6 heterojunction photocatalysts by a two-step solvothermal process followed by annealing at elevated temperature. The catalysts showed superior activity compared to neat Bi_2WO_6 and Bi_2O_3 for the photodegradation of RhB. The enhancement mechanism of the heterojunction catalysts was also discussed.

* Corresponding author. Fax: +86 20 8711 4099.
E-mail address: zhangwd@scut.edu.cn (W.-D. Zhang).

0022-4596/$ - see front matter © 2011 Elsevier Inc. All rights reserved.
doi:10.1016/j.jssc.2011.05.057

2. Experimental section

2.1. Preparation

All chemicals were of analytical grade and used without further purification. The Bi_2O_3/Bi_2WO_6 catalysts were prepared by a two-step solvothermal process with Bi_2WO_6 as the substrate. Bi_2WO_6 was firstly synthesized as follows: 2.5 mmol $Bi(NO_3)_3 \cdot 5H_2O$ and 1.25 mmol $Na_2WO_4 \cdot 2H_2O$ were dissolved in 18 ml ethylene glycol (EG) with the assistance of ultrasonication for 15 min, and the mixture was continuously stirred for 10 min to form a transparent solution. Subsequently, ethanol (18 ml), formaldehyde (4 ml) and urea (7.5 mmol) were added, and a lot of white precipitates appeared. The mixture was stirred for another 20 min and then transferred into a Teflon-lined autoclave (50 ml in volume). The autoclave was sealed and heated at 160 °C for 12 h. After being cooled down to room temperature naturally, the products were collected by filtration, washed by distilled water and dried at 60 °C overnight.

For the synthesis of Bi_2O_3/Bi_2WO_6, desired amount of bismuth nitrate ($Bi(NO_3)_3 \cdot 5H_2O$) was dissolved in 13 ml ethylene glycol and 27 ml ethanol, and then ultrasonicated until the solution became clear. 0.2 g Bi_2WO_6 powders were added into the solution and stirred for 30 min. The mixture was then transferred into a Teflon-lined autoclave, sealed and heated at 160 °C for 5 h. After being cooled down to room temperature naturally, the products were collected by filtration, washed with water and dried at 60 °C. Finally, the precursor was calcined at 400 °C for 2 h. As a reference, Bi_2O_3 powders were synthesized by the same procedure without adding Bi_2WO_6.

2.2. Characterization

The crystalline structure of the products was examined by an X-ray diffractometer (XRD, Bruke-D8, with Cu*K*α radiation). The morphology of the samples was observed by scanning electron microscopy (SEM, JSM-6380-LA, JEOL, Japan) and transmission electron microscopy (TEM, JEOL JEM2010). X-ray photoelectron spectroscopy (XPS) using a Model VG ESCALAB apparatus with Al*K*α X-ray source was employed to analyze the surface composition of the catalysts. The binding energies are calibrated with respect to the signal for adventitious carbon (binding energy = 284.6 eV). UV–vis diffuse reflectance spectroscopy (UV–vis DRS) absorption spectra were recorded at a UV-2550 spectrophotometer in the wavelength range of 200–800 nm. Brunauer–Emmett–Teller (BET) surface area was determined by nitrogen adsorption (Micromertics ASAP 2000 system).

2.3. Photocatalytic test

The catalysts were evaluated by photocatalytic decolorization of rhodamine B (RhB) under irradiation of visible light ($\lambda > 420$ nm). A 300 W tungsten halide lamp (Foshan electric light Ltd.) was used as the light source with a 420 nm cutoff filter to provide visible light irradiation. Experiments were performed at ambient temperature (25 °C). For the degradation of RhB, 0.10 g of the prepared photocatalyst was added into 100 ml of RhB solution (10^{-5} mol l^{-1}). Before illumination, the suspensions were stirred for 30 min in dark in order to ensure the establishment of an adsorption–desorption equilibrium between the photocatalyst and the RhB. Then, the solution was exposed to visible light irradiation under magnetic stirring. At 1 h intervals, 6 ml solution was sampled. The concentration of RhB was determined by measuring the UV–vis spectra every certain time.

3. Results and discussion

3.1. Characterization of the photocatalysts

Fig. 1 displays the XRD patterns of the Bi_2O_3/Bi_2WO_6 samples. The orthorhombic Bi_2WO_6 (JCPDS No. 39-0256) and monoclinic Bi_2O_3 (JCPDS No. 41-1449) were obtained for the single phase samples. In the composites, tetragonal Bi_2O_3 (JCPDS No. 65-1209) and orthorhombic Bi_2WO_6 (JCPDS No. 39-0256) are formed. The samples do not exhibit any Bi_2O_3 diffraction characteristic until its content reaches 10 wt%, which confirms the small nanoparticle size and high dispersion degree. No significant shifts of the principal diffraction peaks were observed, indicating the Bi_2O_3 exists as a separate phase rather than being incorporated into the Bi_2WO_6 lattice.

Fig. 2 shows quantitative XPS analysis on 3 wt% Bi_2O_3-loaded Bi_2WO_6 after thermal treatment at 400 °C for 2 h. The typical full survey and high-resolution spectra for Bi 4*f*, W 4*f*, and O 1*s* region are indicated in Fig. 2A. One can see that the sample contains only C, O, Bi, and W elements. Carbon can be ascribed to the adventitious hydrocarbon from XPS instrument itself. High resolution XPS spectrum of Bi 4*f* region is shown in Fig. 2B. The peaks centered at 164.0 and 158.6 eV are assigned to Bi $4f_{5/2}$ and Bi $4f_{7/2}$, respectively, which demonstrate that all the Bi species in the as-prepared samples are in the form of Bi^{3+}. However, it is worth noting that these binding energy values are not exactly the same as those obtained from pure Bi_2O_3 or Bi_2WO_6 [30,31], which reveals that interfacial structure was formed and the local environment and electron density of the elements changed in some degree. Similarly, the W 4*f* peaks of the sample appear at 36.8 and 34.8 eV (Fig. 2C). These values are also slightly deviant [31], which could be attributed to the existence of Bi_2O_3 too. The O 1*s* band also splits into some contributions, as shown in Fig. 2D, in which three spectra are observed. The peak at 533.3 can be assigned to Bi–O in Bi_2O_3 [30], whereas the peaks located at 529.7 and 531.6 eV, respectively, are ascribed to the oxygen attached to bismuth and tungsten (Bi–O and W–O bonds) in Bi_2WO_6 [24,32]. On the other hand, according to the XPS result (3 wt% Bi_2O_3/Bi_2WO_6), the concentration of the surface Bi^{3+} is 8.8 atom%, whereas that of W^{6+} is 3.29 atom%. The atomic ratio of Bi and W was about 2.67, which is larger than the stoichiometric ratio in Bi_2WO_6. This result reveals the existence of Bi_2O_3 species, which is in good accordance with the conclusion based on the aforementioned XRD result.

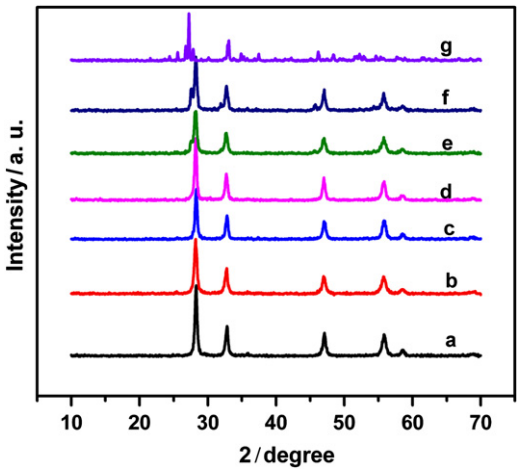

Fig. 1. XRD patterns of (a) Bi_2WO_6, (b) 1 wt% Bi_2O_3/Bi_2WO_6, (c) 3 wt% Bi_2O_3/Bi_2WO_6, (d) 5 wt% Bi_2O_3/Bi_2WO_6, (e) 10 wt% Bi_2O_3/Bi_2WO_6, (f) 15 wt% Bi_2O_3/Bi_2WO_6, and (g) Bi_2O_3.

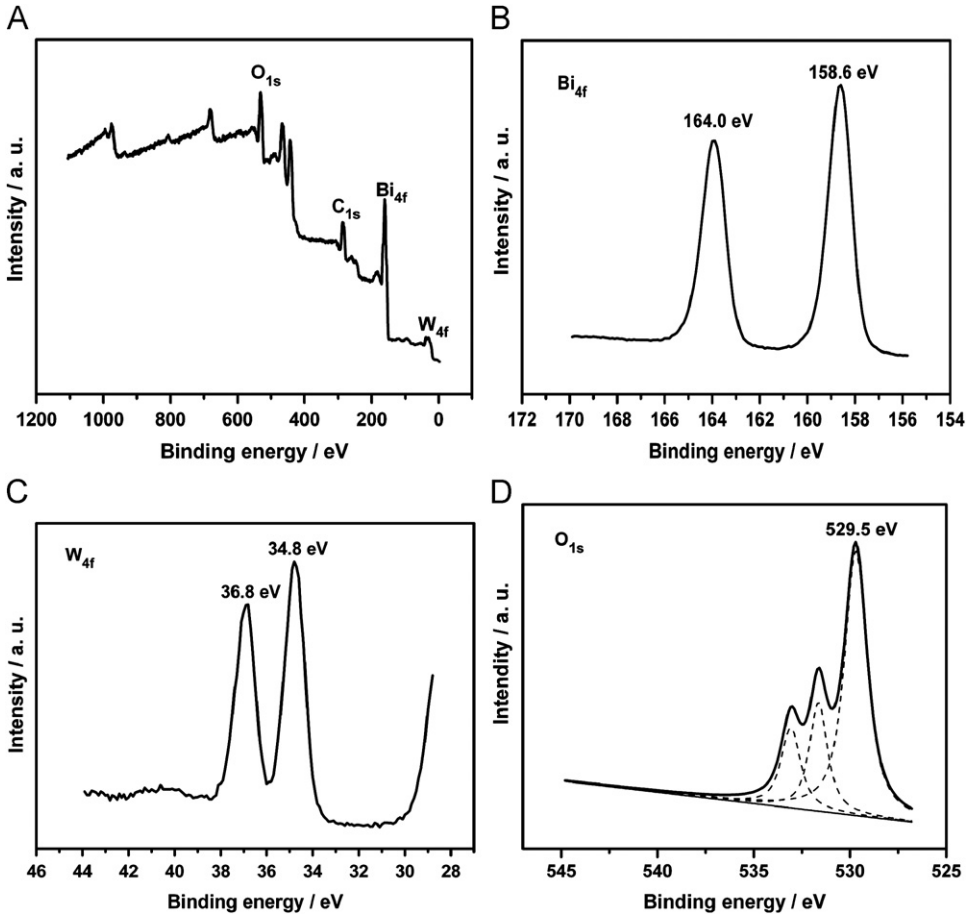

Fig. 2. XPS profiles of the 3 wt% Bi_2O_3/Bi_2WO_6 photocatalyst.

The prepared Bi_2WO_6 and 3 wt% Bi_2O_3/Bi_2WO_6 have similar BET surface areas, which are 27.31 and 25.13 $m^2\ g^{-1}$, respectively.

The morphology of the product was observed by SEM and TEM. As displayed in Fig. 3A, the prepared Bi_2WO_6 exhibits 3D hierarchical structure, which is built from two-dimensional nanoplatelets in a special fashion. After the deposition process and subsequent calcination treatment at 400 °C for 2 h, the Bi_2O_3/Bi_2WO_6 hierarchical structure remains almost unchanged except for the slightly coarse surface (Fig. 3B) compared to the unmodified Bi_2WO_6. To further obtain information about the structure of the sample, the Bi_2O_3/Bi_2WO_6 was characterized by TEM. As shown in Fig. 3C, when 3 wt% Bi_2O_3 is loaded, Bi_2O_3 nanoparticles with a small size of 10–15 nm are tightly coupled on the surface of Bi_2WO_6 even when they are subjected to an ultrasonic treatment. By measuring the lattice fringes, the resolved interplanar distances are 0.272 and 0.319 nm, corresponding to the (0 0 2) plane of Bi_2WO_6 and the (2 0 1) plane of Bi_2O_3, respectively (Fig. 3D). Furthermore, an interconnected fine nanoparticulate morphology was observed, indicating a Bi_2O_3/Bi_2WO_6 nanocrystal heterojunction was formed in the composite catalyst.

As indicated in Section 2, Bi_2O_3 was deposited onto the Bi_2WO_6 microspheres by a solvothermal process using $Bi(NO_3)_3$ as the Bi source and a mixture of EG and ethanol as the solvent. The surface of the Bi_2WO_6 microsphere is hydrophilic and possesses a distribution of OH groups [19]. As a result, EG was firstly absorbed onto the surface of Bi_2WO_6 microspheres by forming hydrogen bonds. Simultaneously, Bi^{3+} and EG formed a relatively stable compound of $Bi_2(OCH_2CH_2O)_3$ because of the strong coordination role of EG (Eq. (1)). Therefore, Bi^{3+} can be successfully absorbed onto the surface of Bi_2WO_6 [33]. Finally, the Bi_2O_3 nanoparticles were obtained through hydrolysis of $Bi_2(OCH_2CH_2O)_3$ (Eq. (2)) [34]:

$$2Bi(NO_3)_3\cdot 5H_2O + 3HOCH_2CH_2OH + 6C_2H_5OH \leftrightarrow Bi_2(OCH_2CH_2O)_3 + 6C_2H_5ONO_2 + 16H_2O \quad (1)$$

$$Bi_2(OCH_2CH_2O)_3 + 3H_2O = Bi_2O_3\downarrow + 3HOCH_2CH_2OH \quad (2)$$

The UV–vis diffuse reflectance spectra of the samples are illustrated in Fig. 4. The absorption of Bi_2WO_6, Bi_2O_3, and Bi_2O_3/Bi_2WO_6 powders starts at about 485, 498, and 545 nm, respectively, which indicates that they are all visible light active semiconductors. The steep shape of the spectra also exhibits that the visible light absorption is not due to the transition from the impurity level but to the band-gap transition of the semiconductors [35]. For a crystalline semiconductor, it shows that the optical absorption near the band edge follows the equation $\alpha(h\nu) = A(h\nu - Eg)^{1/2}$, where α, ν, E_g, and A stand for the absorption coefficient, light frequency, band gap energy, and a constant, respectively [36]. The band gap energy is estimated on the plot $(Ah\nu)^2 = f(h\nu)$ by the intercept of the tangent to the plot with abscissa, which is 2.56, 2.48, and 2.28 eV for Bi_2WO_6, Bi_2O_3, and Bi_2O_3/Bi_2WO_6, respectively. Obviously, loading Bi_2O_3 onto Bi_2WO_6 enhances its visible light absorption. This can be ascribed to the mutual photosensitization of Bi_2O_3 and Bi_2WO_6 [37].

3.2. Photodegradation of organic compounds under visible light irradiation

The photocatalytic activity of the samples was evaluated by decomposing RhB aqueous solution under visible light irradiation.

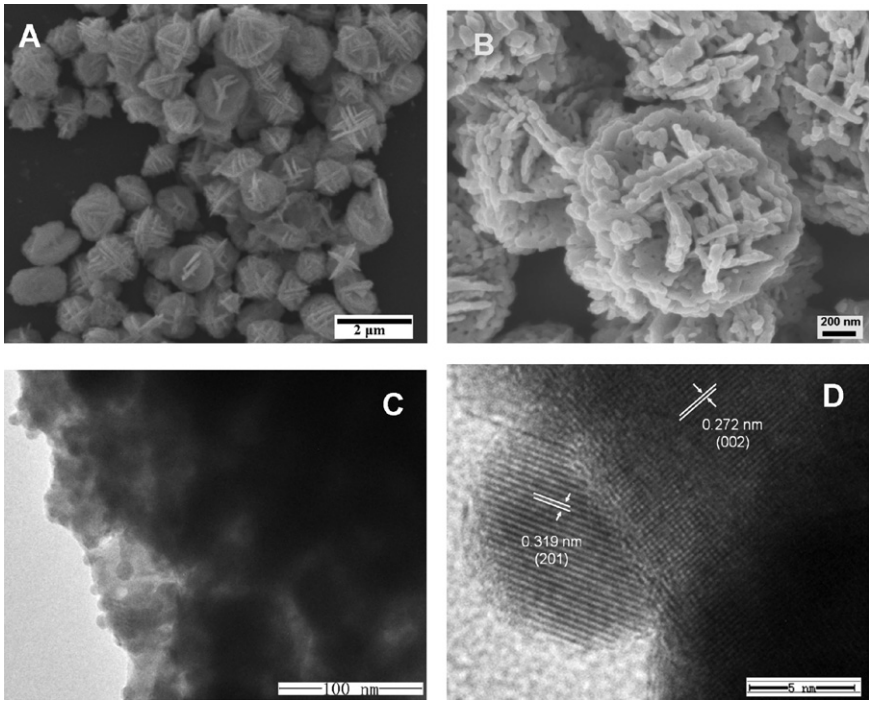

Fig. 3. SEM images of (A) Bi_2WO_6, (B) 3 wt% Bi_2O_3/Bi_2WO_6, and (C and D) TEM images of 3 wt% Bi_2O_3/Bi_2WO_6.

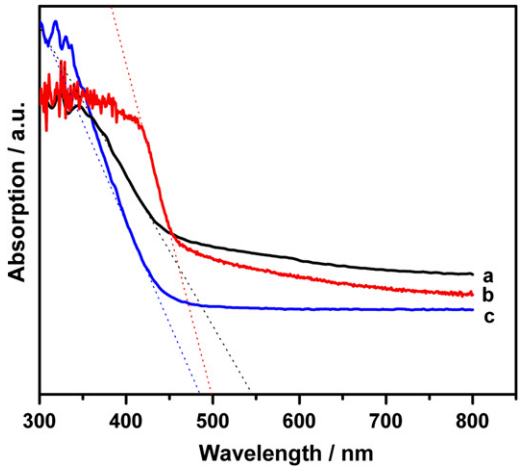

Fig. 4. UV–vis diffuse reflectance spectra of (a) 3 wt% Bi_2O_3/Bi_2WO_6, (b) Bi_2O_3, and (c) Bi_2WO_6.

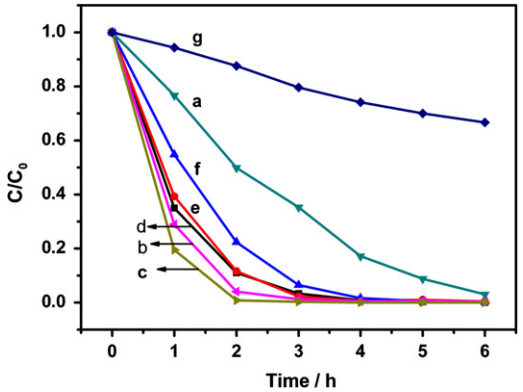

Fig. 5. Effects of the Bi_2O_3 content in the heterojunction catalysts on the degradation of RhB: (a) Bi_2WO_6, (b) 1 wt%, (c) 3 wt%, (d) 5 wt%, (e) 10 wt%, (f) 20 wt%, and (g) Bi_2O_3.

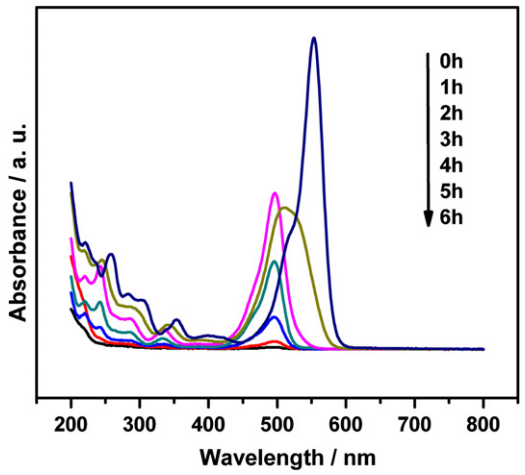

Fig. 6. The temporal evolution of the spectra during the photodegradation of RhB mediated by 3 wt% Bi_2O_3/Bi_2WO_6 under visible light.

Fig. 5 displays the changes of the RhB concentration versus the reaction time over the catalysts with different loading levels of Bi_2O_3. It is observed that compared to pure Bi_2WO_6, the photocatalytic degradation efficiency of RhB increases with the increase of Bi_2O_3 content and reaches an optimum at 3 wt% Bi_2O_3. After that, the activity of the photocatalysts sequentially decreases. It is possible that excessive Bi_2O_3 might reduce surface active sites of Bi_2WO_6. This result demonstrates that in this system, Bi_2O_3 is crucial for getting high performance of the catalysts and the optimum content for the highest catalytic activity is 3 wt% Bi_2O_3. It is noted that the photodegradation of RhB is lower than that reported in Ref. [28]. This can be ascribed to the difference in the light source used. In this study, visible light (>420 nm) was used, while the previous study [28] used the simulated sun light, which contains part of UV.

Fig. 6 depicts the temporal evolution of the spectra during the photodegradation of RhB mediated by the 3 wt% Bi_2O_3/Bi_2WO_6

under visible light irradiation ($\lambda > 420$ nm). After 60 min irradiation, the maximum absorption band of the solution gradually shifted from 554 to 496 nm and the color of RhB aqueous solution changed from pink to light green. Meanwhile, the absorption band gradually decreased, which indicates that the ethyl groups of RhB were removed during irradiation [38–43]. After 2–6 h reaction, the adsorption peak of the dye at around 496 nm underwent a fairly large decrease and the color of dye gradually disappeared with the increase of irradiation time, whereas the hypsochromic shifts of the absorption band are considerably insignificant. It is presumed that the cleavage of the whole chromophore structure (cycloreversion) of RhB occurs over the photocatalysts [42,44]. The result demonstrates that the heterojunction structure of Bi_2O_3/Bi_2WO_6 can improve the catalytic activity to degrade RhB under visible light irradiation.

Although the 3 wt% Bi_2O_3/Bi_2WO_6 microspheres exhibit higher photocatalytic activity, in view of practical application, its stability is very important. To confirm the stability and efficiency of the photocatalytic performance of the Bi_2O_3/Bi_2WO_6, circulating runs in the photocatalytic degradation of RhB under visible light were checked. As shown in Fig. 7, after four terms of recycling, the photocatalytic activity does not exhibit any significant loss, indicating very high stability of the Bi_2O_3/Bi_2WO_6 photocatalyst.

3.3. Reaction mechanism

As is known to all, in a typical photocatalytic procedure, photoinduced holes (h^+_{VB}) and/or the formed hydroxyl radicals ($^{\bullet}OH$) can be extremely active to organic pollutants as a trigger of oxidization [45,46]. Therefore, it is important to detect the main oxidant in the photodegradation process for investigating the photocatalytic mechanism [47,48]. In general, experiments are carried out using EDTA-2Na as a hole scavenger and isopropyl alcohol as a radical scavenger to determine the active species in the photocatalytic reactions [42,49]. In the system containing 3 wt% Bi_2O_3/Bi_2WO_6 photocatalyst, electron–hole pairs were produced under visible-light irradiation, yielding radicals and holes as oxidants. After a reaction of 60 min, the photodegradation process was decelerated distinctively after EDTA-2Na was added and the photodegradation rate was greatly decreased from 83.2% to 39.2%, while the degradation rate of 79.7% was obtained after isopropyl alcohol was added (Fig. 8). This indicates that photogenerated holes are the main oxidants during photocatalytic process.

Based on the above experimental results and discussion, the most plausible mechanism for the degradation of pollutants under visible light irradiation is proposed, as is displayed in Fig. 9. Under visible light irradiation, electrons (e) in the valence bands (VB) were excited to conduction bands (CB), with the same amount of holes (h^+) left in VBs in both Bi_2O_3 and Bi_2WO_6. Then, electrons in the conduction band of Bi_2O_3 were injected into the CB of Bi_2WO_6 because the CB of Bi_2O_3 is more negative than that of Bi_2WO_6. This is beneficial for reducing their recombination. The photogenerated electrons were then captured by O_2 to yield O_2^- and H_2O_2, and then to hydroxyl radicals [50,51]. On the other hand, the photogenerated holes in Bi_2O_3 are powerful oxidative species, which can activate some unsaturated organic pollutants, leading to their subsequent decomposition [52]. The photogenerated holes have been demonstrated to play a major role for the degradation of organic compounds over the Bi_2O_3/Bi_2WO_6 catalysts.

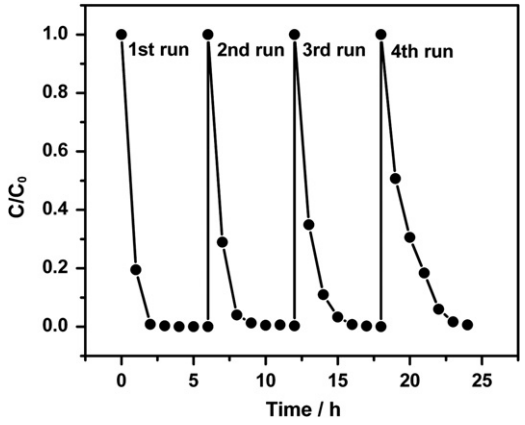

Fig. 7. Cycling runs of the photocatalytic degradation of RhB in the presence of 3 wt% Bi_2O_3/Bi_2WO_6 under visible light.

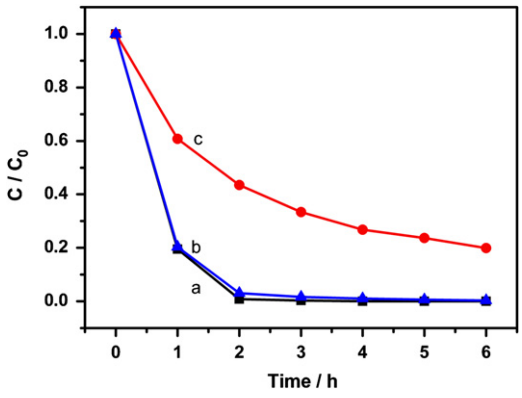

Fig. 8. Photodegradation of RhB over 3 wt% Bi_2O_3/Bi_2WO_6: (a) without radical scavenger, (b) with isopropyl alcohol, and (c) with EDTA-2Na (10^{-3} M).

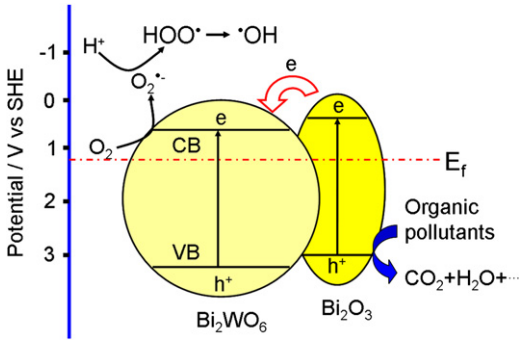

Fig. 9. Schematic diagram of charge separation in a visible light irradiated Bi_2O_3/Bi_2WO_6 heterojunction.

4. Conclusion

In summary, the Bi_2O_3/Bi_2WO_6 heterojunction photocatalysts have been prepared via a two-step solvothermal process followed by annealing at elevated temperature with Bi_2WO_6 as the substrate. This technique is quite simple and environmentally benign. By this approach, a tight chemically bonded interface between the coupled materials can be constructed. The heterojunction catalysts Bi_2O_3/Bi_2WO_6 exhibit higher photocatalytic activity than pure Bi_2WO_6 and Bi_2O_3 for the degradation of RhB under visible light irradiation with an optimal activity at the 3 wt% Bi_2O_3/Bi_2WO_6 catalyst. The remarkable enhancement in the photocatalytic performance of Bi_2O_3/Bi_2WO_6 is ascribed mainly to the Bi_2O_3/Bi_2WO_6 heterojunction, which improves the separation of photogenerated electron–hole pairs. The Bi_2O_3 and Bi_2WO_6 mutual photosensitization caused strong spectral response in the visible region, which is also favorable for the high photocatalytic property. In addition,

a more detailed investigation reveals that the photoinduced holes (h^+_{VB}) are the main active species during the photodegradation process based on the radical and hole trapping experiments. This study provides a new insight for developing novel heterojunction photocatalysts for efficient removal of organic pollutants.

Acknowledgments

The authors thank the National Natural Science Foundation of China (No. 21043005 and No. 20773041) and the Research Fund for the Doctoral Program of Higher Education (No. 20070561008) for the financial support. Q.X. Su would also like to extend her thanks to the Student Research Program of SCUT for the financial aid.

References

[1] A. Fujishima, K. Honda, Nature 238 (1972) 37–38.
[2] X.B. Chen, S.S. Mao, Chem. Rev. 107 (2007) 2891–2959.
[3] D.N. Ke, H.J. Liu, T.Y. Peng, X. Liu, K. Dai, Mater. Lett. 62 (2008) 447–450.
[4] T.C. Jagadale, S.P. Takale, R.S. Sonawane, H.M. Joshi, S.I. Patil, B.B. Kale, S.B. Ogale, J. Phys. Chem. C 112 (2008) 14595–14602.
[5] S.Y. Chai, W.I. Lee, J. Catal. 262 (2009) 144–149.
[6] C.H. Chen, Y.H. Liang, W.D. Zhang, J. Alloy. Compd. 501 (2010) 168–172.
[7] W.D. Zhang, B. Xu, L.C. Jiang, J. Mater. Chem. 20 (2010) 6383–6391.
[8] A. Hameed, P. Fornasiero, Chem. Phys. Lett. 483 (2009) 254–261.
[9] Y. Xu, M.A.A. Schoonen, Am. Mineral 85 (2000) 543–556.
[10] A. Hameed, V. Gombac, T. Montini, P. Fornasiero, J. Am. Chem. Soc. 130 (2008) 9658–9659.
[11] Y. Bessekhouad, D. Robert, J.V. Weber, Catal. Today 101 (2005) 315–321.
[12] Z.F. Bian, J. Zhu, S.H. Wang, Y. Cao, X.F. Qian, H.X. Li, J. Phys. Chem. C 112 (2008) 6258–6262.
[13] X.P. Lin, F.Q. Huang, J. Phys. Chem. C 111 (2007) 18288–18293.
[14] A. Hameed, P. Fornasiero, Chem. Phys. Lett. 472 (2009) 212–216.
[15] M. Shang., W.Z. Wang, J. Phys. Chem. C 112 (2008) 10407–10411.
[16] M. Shang, W.Z. Wang, J. Mater. Chem 19 (2009) 6213–6218.
[17] G.Sh. Li, D.Q. Zhang, Environ. Sci. Technol. 44 (2010) 4276–4281.
[18] J. Ren, W.Z. Wang, Catal. Commun. 10 (2009) 1940–1943.
[19] D.K. Ma, S.M. Huang, J. Phys. Chem. C 113 (2009) 4369–4374.
[20] X.J. Dai, Y.S. Luo, W.D. Zhang, S.Y. Fu, Dalton Trans. 39 (2010) 3426–3432.
[21] Y. Huang, Z.H. Ai, J. Phys. Chem. C 114 (2010) 6342–6349.
[22] L.S. Zhang, W.Z. Wang, Z.G. Chen, L. Zhou, J. Mater. Chem. 17 (2007) 2526–2532.
[23] S.W. Liu, J.G. Yu, J. Solid State Chem. 181 (2008) 1048–1055.
[24] F. Amano, K. Nogami, R. Abe, B. Ohtani, J. Phys. Chem. C 112 (2008) 9320–9326.
[25] R. Shi, G.L. Huang, J. Lin, Y.F. Zhu, J. Phys. Chem. C 113 (2009) 19633–19638.
[26] M. Shang, W.Z. Wang, L. Zhang, H.L. Xu, Mater. Chem. Phys. 120 (2010) 155–159.
[27] J. Ren, W.Z. Wang, S.M. Sun, L. Zhang, J. Chang, Appl. Catal. B l92 (2009) 50–55.
[28] M. Ge, Y. f. Li, L. Liu, Z. Zhou, W. Chen, J. Phys. Chem. C 115 (2011) 5220–5225.
[29] M. Shang, W.Z. Wang, L. Zhang, S.M. Sun, L. Wang, L. Zhou, J. Phys. Chem. C 113 (2009) 14727–14731.
[30] Y. Schuhl, H. Baussart, R. Delobel, M. Le Bras, J. Leroy, L.G. Gengembre, J. Rimblot, J. Chem. Soc., Faraday Trans. 79 (1983) 2055–2069.
[31] J. Wu, F. Duan, Y. Zheng, Y. Xie, J. Phys. Chem. C 111 (2007) 12866–12871.
[32] Y. Wang, Y. Wang, Y. Meng, H. Ding, Y. Shan, X. Zhao, X. Tang, J. Phys. Chem. C 112 (2008) 6620–6626.
[33] M. Shang, W.Z. Wang, H.L. Xu, Cryst. Growth Des 9 (2009) 991–996.
[34] Y. Wang, S.K. Li, X.R. Xing, F.Z. Huang, Y.H. Shen, A.J. Xie, X.F. Wang, J. Zhang, Chem. Eur. J. (2011). doi:10.1002/chem.201001846.
[35] T. Saison, N. Chemin, C. Chaneác, O. Durupthy, V. Ruaux, L. Mariey, F. Maugé, P. Beaunier, J.P. Jolivet, J. Phys. Chem. C 115 (2011) 5657–5666.
[36] X. Zhang, Z.H. Ai, F.L. Jia, L.Z. Zhang, J. Phys. Chem. C 112 (2008) 747–753.
[37] N. Serpone, E. Pelizzetti, Photocatalysis: Fundamentals and Application, Edition, Wiley/Interscience, New York, 1989, p. 123.
[38] C. Zhang, Y. Zhu, Chem. Mater 17 (2005) 3537–3545.
[39] T.X. Wu, G.M. Liu, J.C. Zhao, J. Phys. Chem. B 102 (1998) 5845–5851.
[40] T. Watanabe, T. Takizawa, K. Honda, J. Phys. Chem. 81 (1977) 1845–1851.
[41] T. Takizawa, T. Watanabe, K. Honda, J. Phys. Chem. 82 (1978) 1391–1396.
[42] J.D. Zhuang, W.X. Dai, P. Liu, Langmuir 26 (2010) 9686–9694.
[43] J.G. Yu, G.P. Dai, B.B. Huang, J. Phys. Chem. C 113 (2009) 16394–16401.
[44] K. Yu, S.G. Yang, H. He, C. Sun, C.G. Gu, Y.M. Ju, J. Phys. Chem. A 113 (2009) 10024–10032.
[45] N. Serpone, A.V. Emeline, Res. Chem. Intermed. 31 (2005) 391–432.
[46] S.S. Soni, M.J. Henderson, J.F. Bardeau, A. Gibaud, Adv. Mater. 20 (2008) 1493–1498.
[47] S.B. Zhu, T.G. Xu, H.B. Fu, J.C. Zhao, Y.F. Zhu, Environ. Sci. Technol. 41 (2007) 6234–6239.
[48] H. Zhang, R.L. Zong, J.C. Zhao, Y.F. Zhu, Dramatic visible photocatalytic degradation performances due to synergetic effect of TiO_2 with PANI, Environ. Sci. Technol. 42 (2008) 3803–3807.
[49] H. Zhang, R.L. Zong, Y.F. Zhu, J. Phys. Chem. C 113 (2009) 4605–4611.
[50] A. Fujishima, T.N. Rao, D.A. Tryk, J. Photochem. Photobiol. C: Photochem. Rev. 1 (2000) 1–21.
[51] S. Sakthivel, H. Kisch, Angew. Chem. Int. Ed. 42 (2003) 4908–4911.
[52] G.C. Xiao, X.C. Wang, D.Z. Li, X.Z. Fu, J. Photochem. Photobiol. A: Chem. 193 (2008) 213–221.